Automatic algorithm for triaxial hodogram source location in downhole acoustic emission measurement

doi: 10.1190/1.1442677

GEOPHYSICS, VOL. 54, NO. 4 (APRIL 1989); P. 508–513, 9 FIGS.

Automatic algorithm for triaxial hodogram source location in downhole acoustic emission measurement

K. Nagano*, H. Niitsuma*, and N. Chubachi*

ABSTRACT

An automatic acoustic emission (AE) source location algorithm has been developed for downhole AE measurement of subsurface cracks by using the triaxial hodogram method. The *P*-wave arrival time is detected by analyzing crosscorrelation coefficients among three components of AE signal energy; the *P*-wave direction is determined by the method of least squares. For detection of *S*-wave arrival time, a maximum-likelihood method analyzes a distribution of instantaneous values of the *SH*-wave component amplitude.

This algorithm can locate an AE source as accurately as human analysis. For field measurements, it takes less than 4 s to locate an AE source using a 16-bit personal computer with a program in C language. Automatic AE source location by the triaxial hodogram method has been realized with this algorithm.

INTRODUCTION

Downhole acoustic emission (AE) techniques are used in geotechnical areas in order to monitor subsurface crack extensions (Hardy, 1984). Hydraulically induced cracks have been measured and mapped by AE analysis in hot dry rock geothermal projects (Albright and Pearson, 1982; Baria and Green, 1986). Structures and dynamics of natural hydrothermal reservoirs have been revealed by AE analysis (Niitsuma et al., 1985a); and the AE technique has been used for reservoir control in a geothermal power plant (Niitsuma et al., 1985b). The technique is also used for prediction of rock burst in deep mines (Leighton, 1980; Brink and O'Connor, 1983) and for instability monitoring in underground gas storage reservoirs (Hardy and Mowrey, 1984).

A real-time computer-based AE source locating system is necessary when the AE data are used for prediction or control of subsurface crack extensions. Two types of source location methods have been used in subsurface AE measurements. One is a multiple single-element transducer array approach, where traveltime differences for an AE wave among transducers are analyzed; another is a triaxial hodogram method, where three-dimensional (3-D) particle motion is detected by a single three-component downhole transducer to obtain the triaxial hodogram (Albright and Pearson, 1982). The triaxial hodogram method has a particular advantage in geothermal applications and deep-hole measurements because AE source location can be accomplished by single-hole instrumentation. However, three parameters, *P*-wave and *S*-wave arrival times and *P*-wave direction, must be precisely detected, while detection of only *P*-wave arrivals, sometimes including detection of *S*-wave arrivals, is sufficient in the multiple-transducer array method. This fact makes it difficult to realize an automatic analysis system for the triaxial hodogram source location.

Recently the downhole triaxial measurement technique has been used in vertical seismic profiling (VSP), where the triaxial hodogram is examined (Roberts and Crampin, 1986; Stephan, 1985). It is important to develop automatic detection systems for *P* waves and *S* waves in these applications.

An automatic *P*-wave detection method, where short-term and long-term averages of the signal level are examined, was proposed by Allen (1978). Autoregressive (AR) modeling methods for *P*-wave detection have been investigated by Tjøstheim (1975), Shirai and Tokuhiro (1979), Morita and Hamaguchi (1981), and Yokota et al. (1981). Shirai and Tokuhiro (1979), Morita and Hamaguchi (1981), and Yokota et al. (1981) have also applied their methods to *S*-wave detection.

These methods, however, cannot be applied directly to the triaxial hodogram analysis of downhole AE data because (a) a detection error in the *P*-wave arrival will severely affect the estimated *P*-wave direction, (b) an algorithm must deal with signals whose components arrive simultaneously (various modes of waves arrive successively in a wide-band AE signal), and (c) the algorithm must be computationally simple enough to run on a compact computer in the field. Since it cannot detect accurately the onset of a *P* wave, Allen's method cannot be used for triaxial hodogram data because of reason (a). The AR model methods do not lend themselves to realization by an automatic system that uses a small computer; furthermore, they assume simultaneously arriving signals. Except for the system in Western Deep Levels (Brink and O'Connor, 1983),

Manuscript received by the Editor August 13, 1987; revised manuscript received September 15, 1988.
*Faculty of Engineering, Tohoku University, Aramaki aza Aoba, Sendai 980, Miyagi prefecture, Japan.

where very high-quality AE signals can be detected, an automatic system for triaxial hodogram source location has not yet been developed.

This paper describes for the triaxial hodogram method a newly developed automatic AE source location algorithm, which automatically detects *P*-wave arrival time, *P*-wave direction, and *S*-wave arrival time.

PRINCIPLE OF THE TRIAXIAL HODOGRAM METHOD

Figure 1 shows typical AE waveforms and the hodogram of the *P* wave detected by a downhole AE measurement (Niitsuma et al., 1985a). A linearly polarized hodogram is observed at the arrival of the *P* wave, followed by the disturbed hodogram with arrivals of relected and refracted *P* waves. After that, a high-amplitude *S* wave is observed. The distance between the AE source and observing point L is calculated from

$$L = \Delta T_{ps}/(1/V_s - 1/V_p), \tag{1}$$

where V_p and V_s are *P*-wave and *S*-wave velocities, respectively, and ΔT_{ps} is the arrival-time difference between the *P* wave and the *S* wave. The direction of the AE source is determined from the direction of *P*-wave polarization, assuming the medium is isotropic and homogeneous.

NEW ALGORITHM FOR AUTOMATIC DETECTION OF *P*-WAVE ARRIVAL TIME

In field measurements, various types of AE waveforms are observed depending on the source mechanism, raypath, and distance to the AE source. These variations make it difficult to detect the *P*-wave arrival automatically by a simple threshold level detection.

A new automatic algorithm for the *P*-wave arrival detection, named "component energy comparison method" (CECM), has been developed. In the algorithm, the *P*-wave arrival is detected by examining a difference of accumulated AE signal energy between three components. The difference is represented by crosscorrelation coefficient $R_{xz}(t, T)$,

$$R_{xz}(t, T) = \frac{\frac{1}{T}\sum_{i=t}^{t+T} E_x(i)E_z(i)}{\sqrt{\left(\frac{1}{T}\sum_{i=t}^{t+T} E_x^2(i)\right)\left(\frac{1}{T}\sum_{i=t}^{t+T} E_z^2(i)\right)}}, \tag{2}$$

where E_x and E_z are accumulated signal energy levels of the x and z components such that

$$E_x(t) = \sum_{i=1}^{t} x^2(i)$$

and

$$E_z(t) = \sum_{i=1}^{t} z^2(i),$$

and T is the fundamental period of the *P* wave, which is defined on the basis of prior downhole AE measurement.

This crosscorrelation coefficient changes with time: each component of accumulated AE signal energy increases at the same rate for the random noise preceding the *P*-wave arrival, and the coefficient is almost unity. Except in four special AE source directions, the wave energy of the three components increases at different rates after the *P*-wave arrival, since their respective amplitudes are different. The crosscorrelation coefficient, therefore, decreases at the *P*-wave arrival. After the *P*-wave arrival, the crosscorrelation coefficient returns to unity, because the variation in accumulated energy is small compared to the total accumulated energy and the crosscorrelation coefficient is controlled by the total value. The *P*-wave arrival time is provisionally determined as the time at which the coefficient is minimum as shown in Figure 2a.

After determination of the provisional *P*-wave arrival time, the signal-to-noise ratio (S/N) is examined, where

$$\mathrm{S/N} = 20 \log (P_s/P_n). \tag{3}$$

P_s and P_n in equation (3) are defined as

$$P_s = \frac{1}{T}\sum_{i=T_{p1}}^{T_{p1}+T} \sqrt{x^2(i) + y^2(i) + z^2(i)} \tag{4}$$

and

$$P_n = \frac{1}{T_{p1}}\sum_{i=1}^{T_{p1}} \sqrt{x^2(i) + y^2(i) + z^2(i)}, \tag{5}$$

where T_{p1} is the provisional *P*-wave arrival time. Signal is considered to be noise if the S/N is smaller than a threshold level previously defined.

The *P*-wave arrival time is more precisely determined in the next step. The average μ and the variance σ^2 of the signal

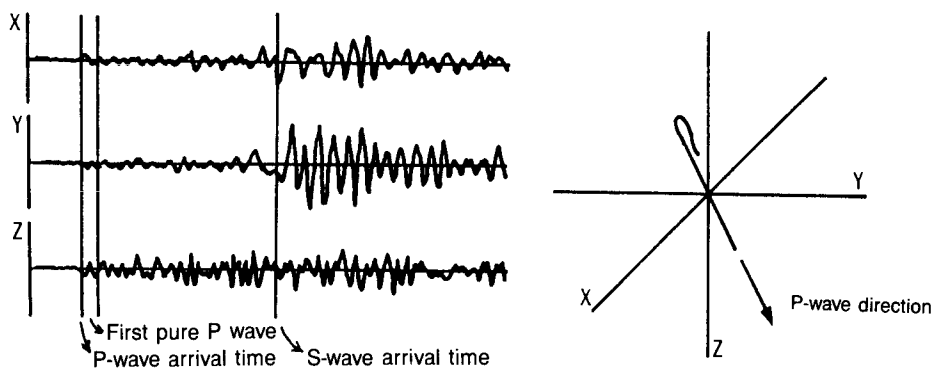

FIG. 1. Parameters which should be detected for the triaxial hodogram location.

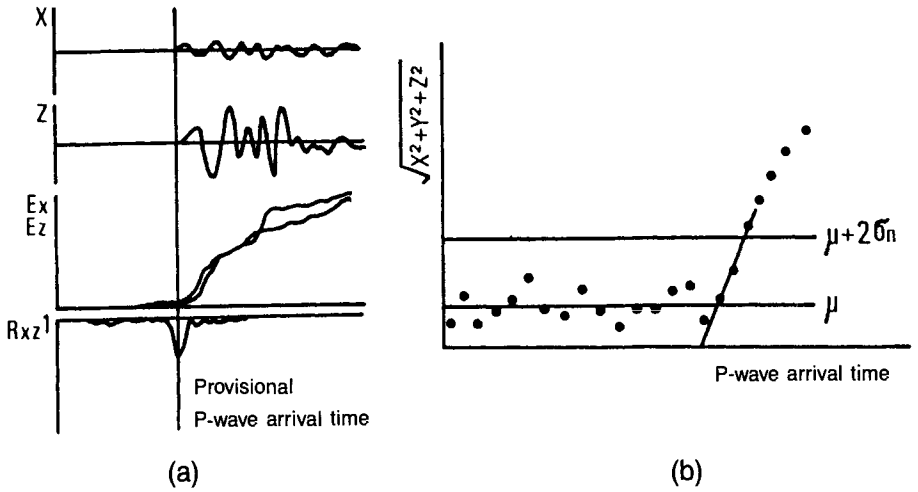

FIG. 2. (a) AE waveforms x, z, accumulated energy levels E_x, E_z, and crosscorrelation coefficient R_{xz}. Provisional P-wave arrival time is the time at which the crosscorrelation coefficient of accumulated energy is minimum. (b) Precise P-wave arrival time is determined by two threshold levels which are defined from average and variance of data prior to the provisional P-wave arrival time.

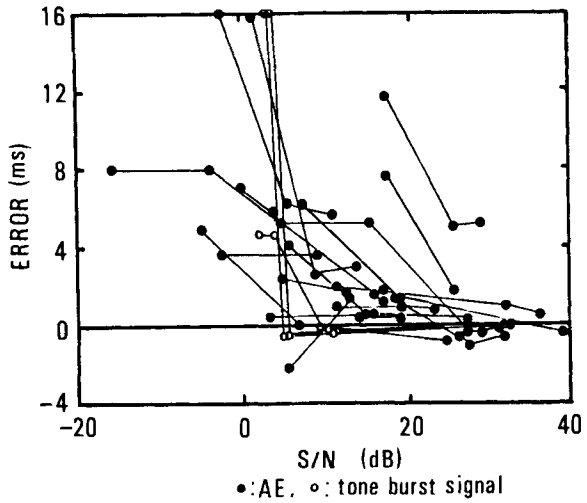

FIG. 3. Computer simulation of the effect of noise on automatic detection of P-wave arrival time. AE signals and tone burst signals, on which Gaussian noise has been superposed, are examined by the P-wave arrival time detection algorithm. Circles connected by a line represent the same signal.

amplitude (the square root of the signal power) are calculated from data before T_{p1}. The signal amplitude between μ and $\mu + 2\sigma$ is approximated by a straight line and the intersection of this line with the time axis is regarded as the P-wave arrival time as shown in Figure 2b. The P-wave arrival time T_p is

$$T_p = t_{p2} - \frac{A_{p2}(t_{p2} - t_{p1})}{A_{p2} - A_{p1}}, \tag{6}$$

where t_{p2} is the time when the signal amplitude exceeds $\mu + 2\sigma$ near T_{p1}; t_{p1} is the time when the signal amplitude exceeds μ before t_{p2}; and A_{p1} and A_{p2} are the signal amplitudes at t_{p1} and t_{p2}, respectively.

The accuracy of the time picked by the algorithm was compared to that from the human analysis for 114 AE events that were detected at Kakkonda geothermal fields during buildup tests of production wells. The digitized AE waveform data were used in this comparison test. The sampling rate and the word size were 5 kHz and 8 bits, respectively; the data length of an AE event was 2048 points/channel. The errors, defined as the differences between automatic and human time picks, of 85 events were within 3 ms. This error corresponds to a distance of about 15 m if the P-wave velocity is 5000 m/s. The algorithm detected the P-wave arrival as well as did humans.

We used a computer simulation, using tone burst signals as well as the actual AE signals to evaluate the effect of noise on the P-wave detection. Gaussian random noise was superposed on the signals. Figure 3 shows the result of the simulation, where the effect of S/N is represented as error between the values determined by the new algorithm and by human analysis of the signal without noise; there is no significant influence of noise when the S/N is higher than 4 dB.

ALGORITHM FOR AUTOMATIC DETECTION OF P-WAVE DIRECTION

Three-dimensional (3-D) least-squares analysis can be applied to the detection of the 3-D P-wave direction. Figure 4 illustrates the algorithm in which a 3-D regression line is the intersection of two planes which are calculated by extending the regression lines of lissajous patterns projected onto the xz and yz planes. The P-wave direction is uniquely determined from the regression line if the AE source is always located below the AE sensor.

In the automatic detection of P-wave direction, it is very important to examine the period of the first pure P wave during which the hodogram is not disturbed by reflected or refracted waves from surface and subsurface boundaries.

An algorithm which detects the pure P-wave period has been devised. The principle is illustrated in Figure 4. A cylindrical threshold level about a distance from the regression line

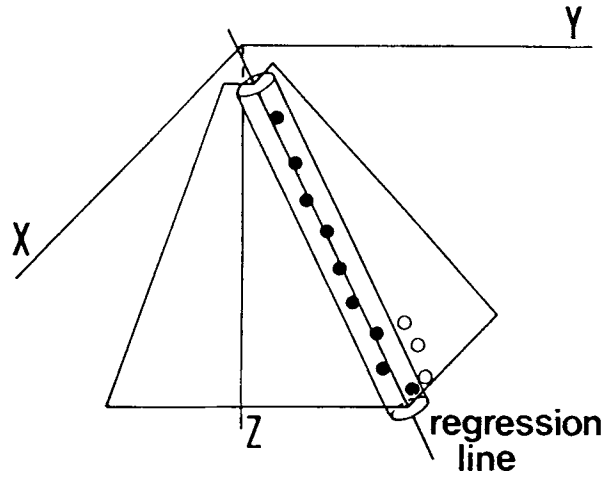

FIG. 4. The principle of detection of *P*-wave direction by the method of least squares. The cylindrical threshold level determines the period of the first pure *P* wave, where a 3-D lissajous pattern of AE data is a straight line.

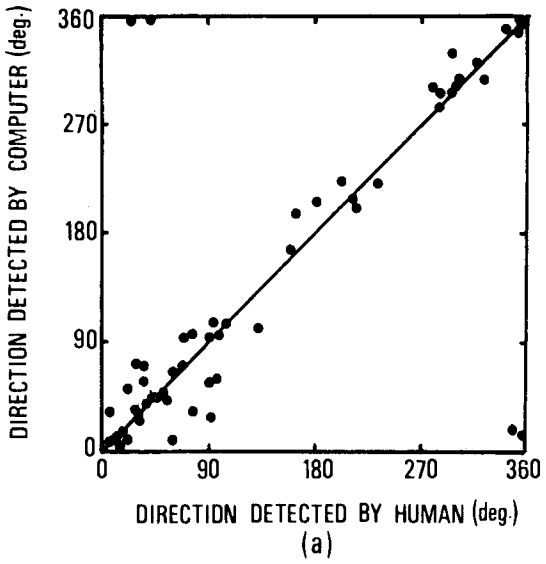

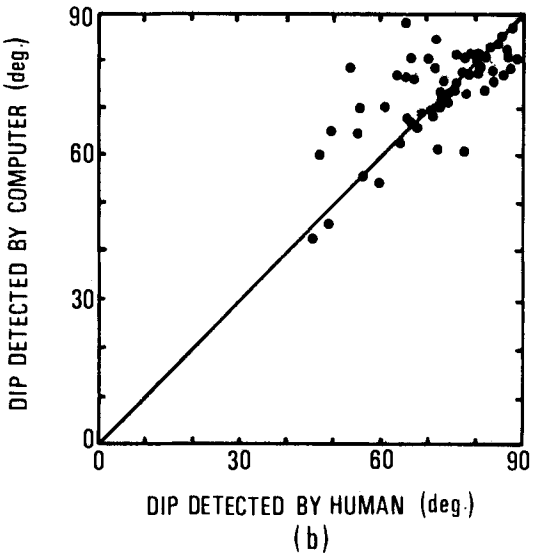

FIG. 5. Comparison of (a) direction and (b) dip detected by human analysis and the automatic algorithm.

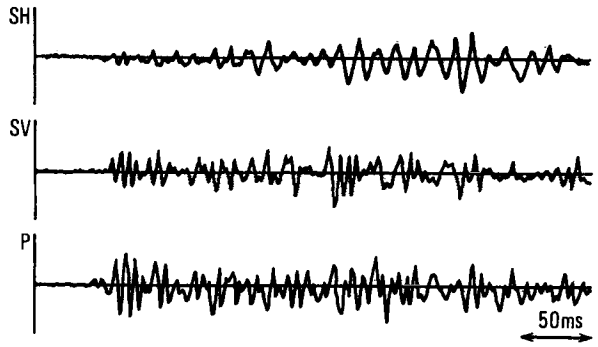

FIG. 6. Examples of *SH*, *SV*, and *P* components of AE waveforms. The *SH* component is more stationary than the *SV* component.

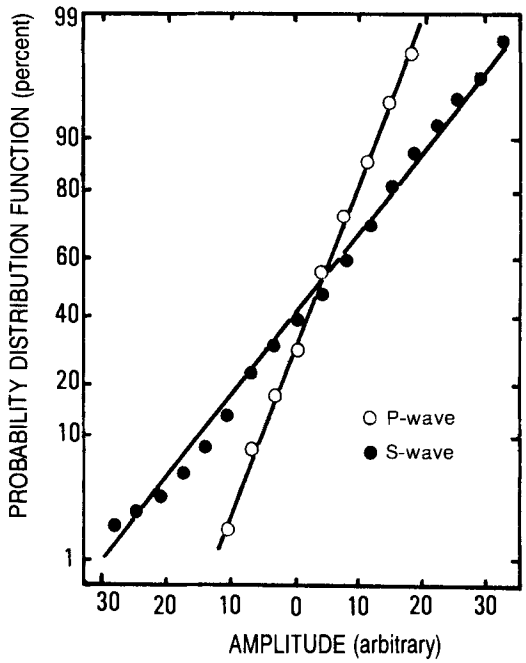

FIG. 7. An example of the probability distribution function of instantaneous values of *P*-wave and *S*-wave amplitudes on the normal probability diagram. The straight line indicates that the instantaneous value data of both waves follow the normal distribution.

is defined. The first regression line is determined during the period sufficiently before the arrival of refracted and reflected waves. When the next data point is inside the cylindrical threshold, a new regression line is calculated from data involving the new point. This procedure is repeated until the calculated number exceeds the threshold.

Comparisons of results by human analysis and the algorithm are shown in Figure 5. The *P*-wave arrival time was detected first by the above mentioned algorithm. For 58 events considered, errors of 39 events are within 10 degrees in direction and errors of 36 events are within 5 degrees in dip as shown in the figure. The period examined for the detection of *P*-wave direction, which is automatically determined in the algorithm, was about a half wavelength in these data.

NEW ALGORITHM FOR AUTOMATIC DETECTION OF *S*-WAVE ARRIVAL TIME

Various waves, which are converted at the subsurface boundaries, are superposed on an AE wave. The property of the signal, therefore, changes with time because of the converted waves, making it difficult to determine the *S*-wave arrival automatically.

The horizontally polarized shear (*SH*) component propagates without mode conversion and is more stationary than other modes which are converted into each other at horizontal subsurface boundaries. Figure 6 shows *SH*, *SV*, and *P* components of an AE signal. The *SH* component is more compact than the others, e.g., than the *SV* component; and the *S*-wave arrival is clearer in the *SH* component. Therefore, the *SH* component is used for the *S*-wave arrival detection.

We have developed a new algorithm for *S*-wave arrival detection, based on an analysis of a probability distribution of instantaneous values of *SH*-component amplitudes. Figure 7 shows an example of the probability distribution of the *P*-wave and *S*-wave amplitudes on a normal probability diagram. Since the distributions are represented as straight lines, both waves have normal probability distributions. Note that the slope of the straight line of the *P* wave is different from that of the *S* wave.

A maximum-likelihood method (Kullback, 1959; Yokota et al., 1981) for the probability distribution of instantaneous values of the *SH* component amplitude is used to detect the *S*-wave arrival time. The AE signal is divided into two stationary models at a dividing time k. Probability density functions $p_p[SH(t)|k]$ and $p_s[SH(t)|k]$ are represented by statistical properties of the *P*-wave and *S*-wave data, respectively. The log likelihood function $\ell[SH(t)|k]$ obtained from equation (9) shows how the two models adapt to the AE signal as a function of k:

$$\ell[SH(t)|k] = \log \prod_{i=1}^{k} p_p[SH(t)|k] \prod_{i=k+1}^{n} p_s[SH(t)|k], \tag{9}$$

where n is the number of data points. The optimum k, i.e., the *S*-wave arrival time, is the time at which $\ell[SH(t)|k]$ is maximum.

When the distribution is normal, the equation takes the simpler form

$$\ell[SH(t)|k] = -\frac{k}{2}\log\frac{1}{k}\sum_{i=1}^{k}[SH(i)-\mu_p]^2 - \frac{n-k}{2}\log\frac{1}{n-k}\sum_{i=k+1}^{n}[SH(i)-\mu_s]^2, \tag{10}$$

where

$$\mu_p = \sum_{i=1}^{k} SH(i)/k, \qquad \mu_s = \sum_{i=k+1}^{n} SH(i)/(n-k).$$

Figure 8 shows an example of the *SH* component of an AE waveform and $\ell[SH(t)/k]$ given by equation (10). The maximum of $\ell[SH(t)/k]$ corresponds closely to the *S*-wave arrival time. The new algorithm fails to determine the *S*-wave arrival time when the amplitude of the *P* wave is comparable to that of the *S* wave, because the new algorithm estimates only the difference of the amplitude distributions. Comparing this new algorithm to human analysis shows detection errors are within 10 ms for 68 of 84 events. A 10 ms error corresponds to a distance of 30 m, when the velocity of the *S* wave is 3000 m/s.

CONCLUSIONS

The automatic AE source location algorithm for the triaxial hodogram method consists of CECM, the *P*-wave direction detection algorithm, and the maximum-likelihood method for the probability distribution of the instantaneous value of *SH* wave amplitude.

The accuracy of the algorithm was estimated by comparing it with human analysis. Figure 9 shows the distances determined by human analysis and with the algorithm. 57 of 84 AE events have errors within 50 m in the figure, when the velocities of the *P* wave and *S* wave were 5000 m/s and 3000 m/s, respectively.

An automatic AE source location system for the triaxial hodogram method has been realized by using the new algorithm. AE location takes less than 4 s on a 16-bit personal computer using a program written in C and machine languages.

ACKNOWLEDGMENTS

The research described in this paper has been conducted as a course of "Γ-Project" under a "Grant in Aid of Special Distinguished Research" of Japan Ministry of Education, Science and Culture.

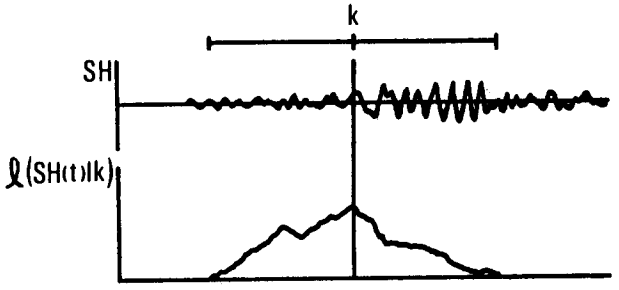

FIG. 8. An example of the log likelihood function of instantaneous values of an *SH* component. The *S*-wave arrival time is the time at which the log likelihood function is maximum.

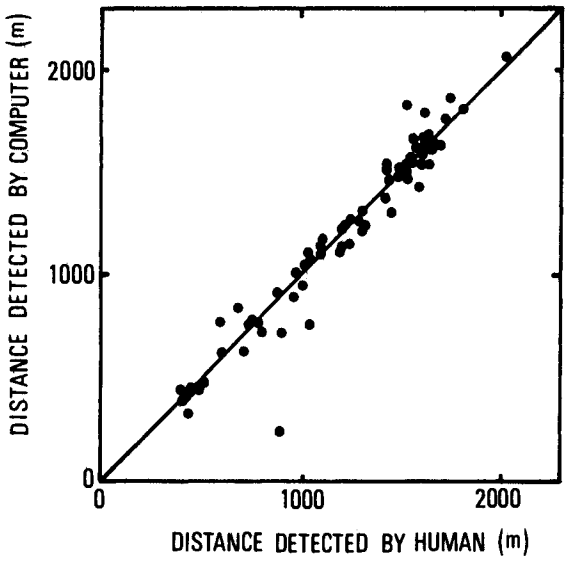

FIG. 9. Comparison of distances detected by human analysis and the automatic algorithm.

REFERENCES

Albright, J. N., and Pearson, C. F., 1982, Acoustic emissions as a tool for hydraulic fracture location: experience at the Fenton Hill Hot Dry Rock Site: Soc. Petr. Eng. J., **22**, 523–530.

Allen, R. V., 1978, Automatic earthquake recognition and timing from single traces: Bull., Seis. Soc. Am., **68**, 1521–1532.

Baria, R., and Green, A. S. P., 1986, Seismicity induced during a viscous stimulation at the Camborne school of mines hot dry rock geothermal energy project in Cornwall, England, *in* Yamaguchi, K., Aoki, K., and Kishi, T., Eds., Progress in Acoustic Emission III: The Japanese Soc. for NDI, 407–429.

Brink, A. V. Z., and O'Connor, D. M., 1983, Research on the prediction of rockbursts at Western Deep Levels: J. S. African Inst. Min. Metall., **65**, 1–10.

Hardy, H. R., Jr., 1984, Geotechnical applications of acoustic emission techniques: present status and future goals, *in* Onoe, M., Yamaguchi, K. and Takahashi, H., Eds., Progress in Acoustic Emission II: The Japanese Soc. for NDI, 632–641.

Hardy, H. R., Jr., and Mowrey, G. L., 1984, Analysis of microseismic data from a natural gas storage reservoir, *in* Hardy, H. R., Jr., and Leighton, F. W., Eds., Proc. 3rd Conf. on Acoustic Emission/Microseismic Activity in Geologic Structures and Materials: Trans Tech Publ., 365–392.

Kullback, S., 1959, Information theory and statistics: Wiley and Sons.

Leighton, F., 1980. Microseismic studies at the Henderson mine, *in* Hardy, H. R., Jr., and Leighton, F. W., Eds., Proc. 2nd Conf. on Acoustic Emission/Microseismic Activity in Geologic Structures and Materials: Trans Tech Publ., 227–244.

Morita, Y., and Hamaguchi, H., 1981, Automatic detection of *S*-onset times using two dimensional autoregressive model fitting: J. Seis. Soc. Jap., **34**, 223–240 (in Japanese).

Niitsuma, H., Nakatsuka, K., Chubachi, N., Yokoyama, H., and Takanohashi, M., 1985a, Acoustic emission measurement of geothermal reservoir cracks in Takinoue (Kakkonda) field, Japan: Geothermics, **14**, 525–538.

——— 1985b, Downhole AE measurement of a geothermal reservoir and its application to reservoir control, *in* Hardy, H. R., Jr., and Leighton, F. W., Eds., Proc. 4th Conf. on Acoustic Emission/Microseismic Activity in Geologic Structures and Materials, to be published.

Roberts, G., and Crampin, S., 1986, Shear-wave polarizations in a hot dry rock geothermal reservoir: anisotropic effects of fractures: Internat. J. Rock Mech. Min. Sci. and Geomech., **23**, 291–302.

Shirai, K., and Tokuhiro, I., 1979, Detection of seismic wave onsets: J. Seis. Soc. Jap., **32**, 141–147 (in Japanese).

Stephan, R. A., 1985, Seismic anisotropy in the upper oceanic crust: J. Geophys. Res., **90**, 11383–11396.

Tjøstheim, D., 1975, Autoregressive representation of seismic *P*-wave signals with an application to the problem of short-period disriminants: Geophys. J. Roy. Astr. Soc., **43**, 269–291.

Yokota, T., Zhou, S., Mizoue, M., and Nakamura, I., 1981, An automatic measurement of arrival time of seismic waves and its application to an on-line processing system: Bull. Earthquake Res. Inst., **55**, 449–484 (in Japanese).